

SENSITIVITY OF A SHOCK-BOUNDARY LAYER INTERACTION TO GEOMETRIC PERTURBATIONS

David B. Helmer

Department of Mechanical Engineering Department of Mechanical Engineering
Stanford University

488 Escondido Mall Building 500, Stanford, CA 94305 lcampo@stanford.edu
dhelmer@stanford.edu

Laura M. Campo

Stanford University

John K. Eaton

Department of Mechanical Engineering
Stanford University
eatonj@stanford.edu

ABSTRACT

2D Particle Image Velocimetry (PIV) was used to study the sensitivity of the shock-boundary layer interaction (SBLI) generated by a small 20° compression ramp in a low aspect ratio continuously operated wind tunnel. A PIV survey of the unperturbed case was taken. The size of the wedge influenced the interaction, which was weaker than that observed in the case of a large compression wedge. Geometric perturbations were introduced upstream of the compression wedge on the opposite wall. Significant changes were observed in the interaction zone, with the system sensitivity a strong function of position in the interaction.

INTRODUCTION

The shock-boundary layer interaction (SBLI) has been an active area of research in fluid mechanics for decades due to its rich physics and relevance to real systems. The interaction is inherently three-dimensional, and these effects are more pronounced in physical systems with low aspect ratios. As with any supersonic flow, these systems are very sensitive to perturbations, and quantification of this sensitivity is key in the development of truly predictive simulations.

Experimental investigations of the SBLI date back to the 1950s. A summary of the early experimental work can be found in Dolling (2001). A variety of techniques have been applied to the study of the SBLI, including the use of fast-response pressure transducers (e.g. Beresh et al. (2002)), hot-wire anemometry (Smits and Muck 1987), filtered Rayleigh scatter, and oil surface flow visualizations (Bookey et al. 2005). A number of recent studies have applied various forms of particle image velocimetry (PIV) to the problem, including standard PIV (e.g. Humble et al. (2007), Ganapathisubramani et al. (2007), Hou et al. (2003), and Piponniau et al (2009)), dual-plane PIV (Souverein et al 2010), and tomographic PIV (Humble et al. 2009).

While the SBLI has been studied extensively, relatively

few studies have evaluated the effect of perturbations on these systems. Some recent studies have evaluated the effect of modifying the boundary conditions in an effort to control the interaction zone. One such study was conducted by Souverein and Debieve (2010), in which air jet vortex generators were used to alter the boundary layer structure. Selig and Smits (1991) studied the effect of periodic blowing on supersonic turbulent boundary layers and the SBLI. Another example is the work of Blinde et al. (2009), in which microramps were placed upstream of an interaction to alter the incoming boundary layer structure. While these studies used small changes in the boundary layer to alter the flow, they focused on controlling the interaction rather than studying its sensitivity.

As an increased emphasis is placed on predictive simulations, a library of validation data is needed to evaluate the ability of these simulations to predict the sensitivity of a given flow configuration to deviations from nominal conditions. The current experiment was designed and performed in parallel with a RANS simulation effort aimed at evaluating uncertainty quantification techniques for CFD. A low aspect ratio, continuously operated Mach 2.05 wind tunnel with a short 20° compression wedge was chosen because the full configuration can be represented in a three-dimensional steady RANS calculation. A deformable wall segment was included in the tunnel to impose a wide range of controlled three-dimensional geometric perturbations. PIV data were collected at the compression corner to evaluate the system response to a range of perturbations.

EXPERIMENTAL SETUP AND DATA PROCESSING

This experiment was performed in a continuously operated Mach 2.05 wind tunnel. The tunnel test section had a 47.5x45.2mm cross section, and the top and bottom walls were made of plexiglass to allow optical access for the laser while the sidewalls were made of black anodized aluminum to

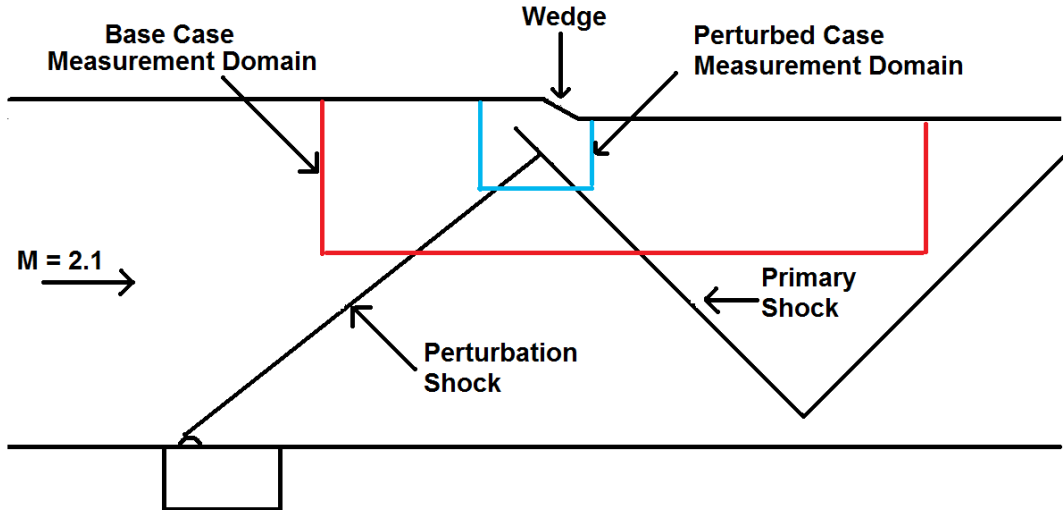


Figure 1. Tunnel Schematic

eliminate reflections. A 15cm plexiglass window was flush-mounted in the sidewall near the compression corner to provide optical access for the camera. A small (3mm long), full-span 20° compression wedge was placed on the top wall 325mm downstream of the end of the nozzle. The tunnel was fed continuously by an Ingersoll Rand SSR-XF400 compressor. The stagnation temperature upstream of the nozzle was kept between 29°C and 31°C at all times, while the upstream stagnation pressure was held within 1% of 154kPa.

The perturbation generator was placed in the bottom wall of the wind tunnel such that deformations could be placed $\approx 25 - 55\text{mm}$ upstream of the compression wedge location. Five slots were machined into the bottom wall, and a $1/16''$ rubber sheet was flush-mounted above them. A 5×5 array of 2.2 mm diameter screws was placed in a low-pressure chamber under the rubber sheet and was mounted on a micrometer traverse. The screws could be individually raised and lowered, and the low pressure served to pull the rubber onto the screw-head, generating a highly repeatable set of geometric perturbations with a maximum height of $\approx 1\text{mm}$.

Two-dimensional PIV was used to quantify the flow field. A NewWave Solo-200XT dual-pulse PIV laser with a wavelength of 532nm and a pulse rate of 4Hz was used. Images were acquired with a TSI model 630047 PIV camera with a 1024×1280 pixel array. The image resolution was $\approx 8.4\mu\text{m}/\text{pixel}$, resulting in a field of view of $\approx 8.6 \times 10.8\text{mm}$. The flow was seeded with olive oil droplets using a TSI model 9307-6 Laskin nozzle seeder. Seeder air was provided by an Ingersoll-Rand model 2340 compressor controlled with a Norgren B74G-4AK-AD1-RMG regulator. Seed was injected upstream of the flow straighteners to encourage a uniform seed distribution and to avoid disturbing the flow downstream of the nozzle. The nominal particle size was $1\mu\text{m}$, resulting in a nominal Stokes number of $\mathcal{O}(0.1)$. The interframe time was set at 800ns, resulting in maximum particle displacements of approximately 50 pixels. 2500 images were acquired for each perturbation surface configuration to give well-converged ve-

locity statistics.

Data were processed using a cross-correlation algorithm written at Stanford designed for large particle displacements and parallel processing. Background subtraction was used to eliminate reflections, and images were high-pass filtered to eliminate particle blurring near the shock. Slight peak-locking was observed, resulting in a small increase in the uncertainty of the measured velocity ($\approx 1\%$). Vectors were validated using a minimum correlation coefficient of 0.5, a consistency filter comparing neighboring vectors, and a 3σ filter.

1 BASE CASE RESULTS

A detailed PIV survey of the base case was performed, with measurements taken in multiple spanwise planes, including several in the sidewall boundary layer. The results of this survey are discussed in detail in Helmer et al (2011). The streamwise velocity near the channel centerline was found to be $\approx 525\text{m/s}$, giving a Mach number of ≈ 2.05 . The boundary layer thickness upstream of the interaction was determined to be 5.4mm, with a momentum thickness of $\approx 450\mu\text{m}$, corresponding to $Re_\delta \approx 85,000$ and $Re_\theta \approx 7200$. Significant three-dimensional effects were observed, both in the upstream boundary layer and in the interaction region. Figure 2 shows the wall-normal velocity contours for the unperturbed flow near the mid-plane of the tunnel. The contours clearly show the shock structure as the flow encounters the compression corner. The observed primary shock angle of 37° is significantly less than the inviscid prediction of 51° for a Mach 2.05 flow encountering a 20° turn. Similarly, the flow angle behind the shock is approximately 8° rather than 20° . Both of these facts are attributed to the small height of the wedge, which is $\approx 1/5$ the incoming boundary layer thickness. The SBLI allows the sonic line to bend well upstream of the corner, resulting in a maximum angle of less than 20° . This results in a weaker SBLI than is observed in comparable flows in the literature (e.g. Ganapathisubramani et al (2007)), as the influence

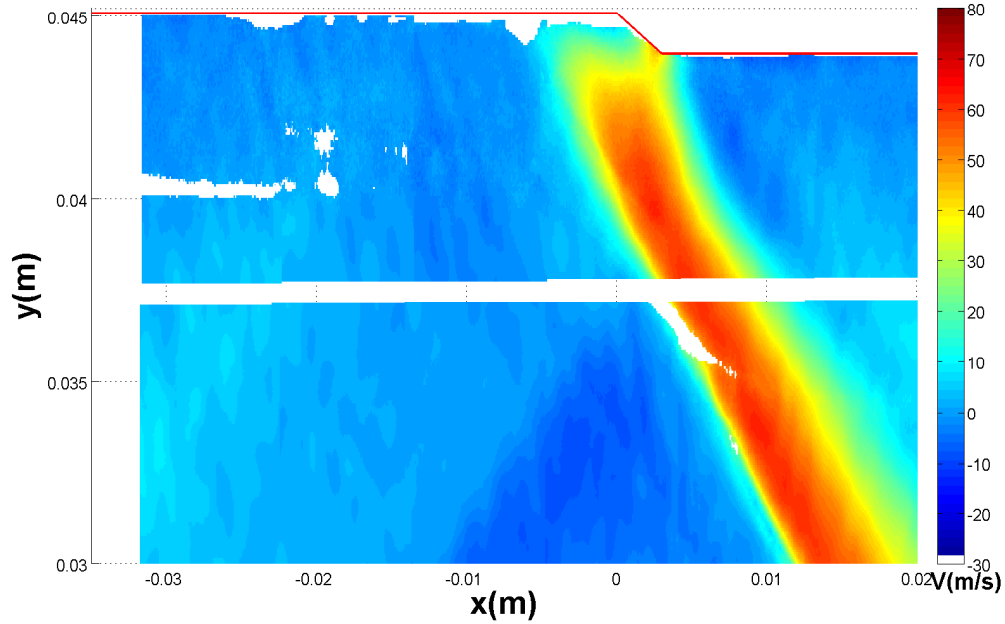


Figure 2. Wall-normal velocity contours of the unperturbed compression corner flow. White regions indicate areas where fewer than 200 valid velocity vectors were found.

of the shock extends only $\approx 2.5\delta$ upstream of the compression corner.

Behind the compression corner, the flow is rapidly turned back toward horizontal by the expansion fan. Because the flow angle near the wedge is 20° , the resulting expansion fan is stronger than the primary shock. As a result, there is a slight velocity component directed towards the wall behind the expansion fan. A weak nozzle shock can be seen impacting the primary shock in the inviscid region - no significant influence on the flow is observed.

2 PERTURBATION RESULTS

It would be impractical to conduct a full survey of the velocity field for each perturbation surface configuration. Instead a single PIV tile was studied for each case, as indicated in Figure 1. This tile was located at the compression corner near the tunnel centerline. This region was expected to be sensitive to perturbations, and includes the primary shock structure.

Twenty-five different perturbed cases were tested in this study. For each case, a spanwise row of five screws was elevated at a given streamwise location, providing a roughly two-dimensional perturbation. Five streamwise locations for the perturbation were studied, with five different bump heights at each location. Figure 3 shows a comparison of the base case flow at the corner to a series of perturbed cases. Several changes are observed in the flow as a result of the perturbation. The most obvious is the presence of the perturbation shock. This shock can be observed as a jump in the wall-normal velocity, and is represented by the leading edge of the dark blue contours in Figure 3. A weak shock is also generated by the leading edge of the perturbation device, and is

indicated with an arrow in the top left plot of Figure 3. The strength of the perturbation shock is a function of the perturbation height, with larger bumps generating stronger shocks. The primary shock moves upstream in the perturbed cases relative to the unperturbed case, indicating a larger interaction region. The flow turning angle is reduced in the perturbed cases, which is consistent with a larger interaction zone that allows more gradual deformation of the sonic line and a weaker primary shock structure. Considering the streamwise velocity contours (Figure 4) shows that the interaction zone is slightly thicker in the perturbed cases. This can be observed by considering the dark blue contours, which are noticeably thicker for the cases with a stronger perturbation shock.

A more quantitative assessment of the system sensitivity can be made by considering the change in the measured velocity profiles at a given streamwise location. Figures 5 and 6 show streamwise velocity profiles at the wedge location and 3mm downstream of the wedge. These profiles show that the system sensitivity is a strong function of position. A different perturbation configuration generates the largest changes for the two locations. In addition, more of the perturbation configurations have noticeable effects on the boundary layer structure for the more downstream location. Near the wall, the perturbations are observed to have minimal influence, as the wedge dominates the flow dynamics. Further from the wall, some perturbations are seen to significantly alter the flow, with peak changes in the velocity of more than 50m/s. This is significantly larger than the velocity drop due to the perturbation shock, which is less than 25m/s. The streamwise velocity contours show the reason for this discrepancy: the perturbed cases show a significantly thicker low-velocity interaction zone even though the perturbation shock impinges on the primary shock rather than the incoming boundary layer.

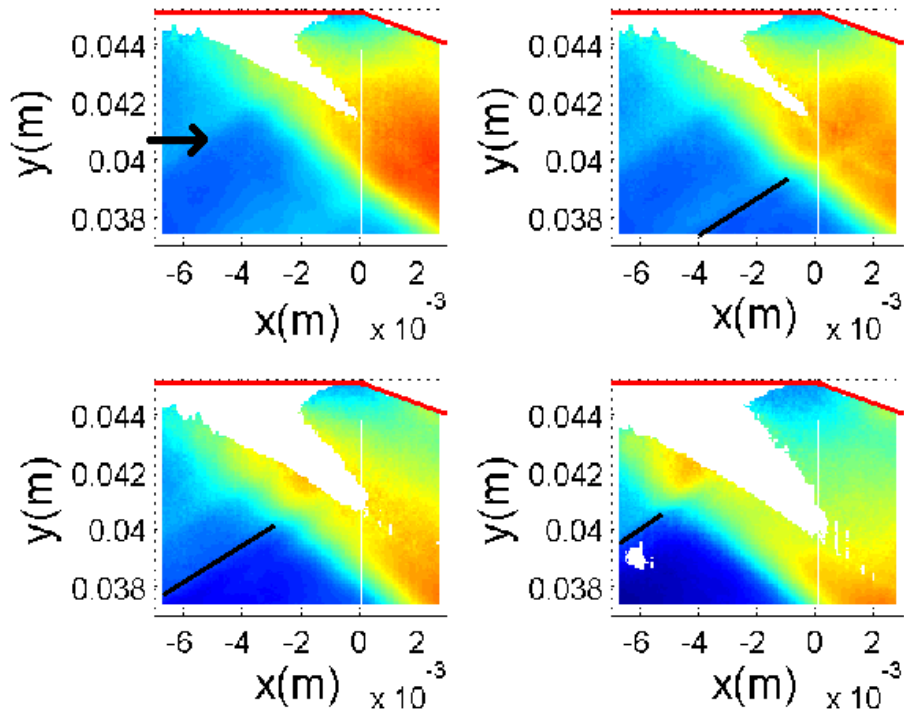


Figure 3. Wall-normal velocity contours - Top left is unperturbed flow. White regions indicate areas where fewer than 200 valid velocity vectors were obtained. Contour levels are the same as Figure 2. Cases shown are for perturbations placed 54.2mm upstream of corner for heights up to ≈ 1 mm. Arrow indicates shock from leading edge of perturbation device. Black lines indicate perturbation shocks.

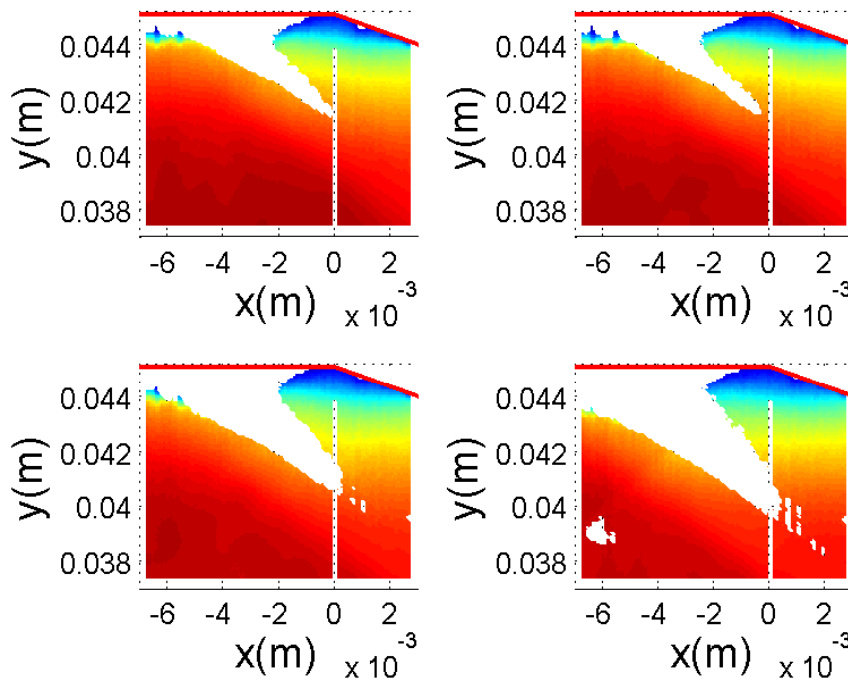


Figure 4. Streamwise velocity contours - Top left is unperturbed flow. White regions indicate areas where fewer than 200 valid velocity vectors were obtained.

This thickening indicates a stronger interaction, as does the increased upstream influence of the wedge. However, the jump in wall-normal velocity across the primary shock does not appear to change significantly, as it is roughly 65-70m/s for all cases, both perturbed and unperturbed, indicating that the primary shock strength is not significantly different.

The flow sensitivity is a strong spatial function, and depends strongly on the size and location of the geometric perturbations. As seen in Figure 5, minimal changes were observed for the majority of the cases examined. However, large changes in the velocity field were seen for the most upstream perturbation location, particularly for the largest perturbation. This suggests that even greater effects could be observed by moving the perturbation further upstream such that the perturbation shock impacts at or near the start of the SBLI.

An additional method for quantitative evaluation of the data can be found by isolating a single location in space. For example, if only the data 1mm from the wall is selected from Figure 5, a histogram representing the system response at that location to perturbations can be extracted. This histogram is shown in Figure 7. This location shows moderate sensitivity to perturbations, with the perturbations causing peak differences of nearly 50m/s in the streamwise velocity. With more samples, this histogram would become an experimental pdf. This pdf can be directly compared to the output of a stochastic simulation and used to validate uncertainty quantification techniques for CFD and simulation predictions of sensitivity.

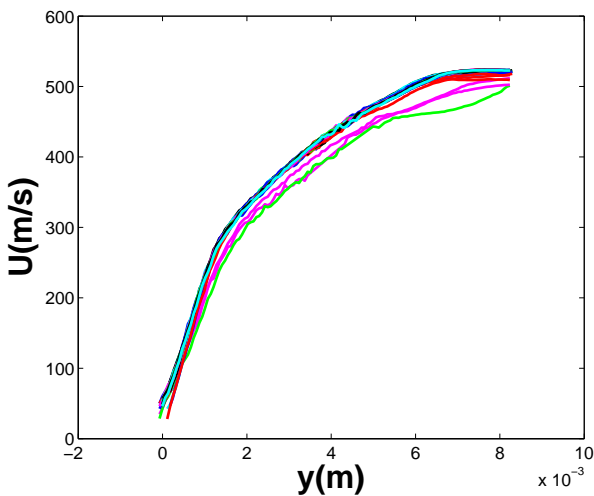


Figure 5. Velocity profiles at the compression corner location for 25 perturbed cases

3 CONCLUSION

The sensitivity of the shock-boundary layer interaction was evaluated in a Monte Carlo-type experiment to provide a validation dataset for simulations using uncertainty quantification techniques. Planar PIV was used to quantify the flow field in a Mach 2.05 continuously operated wind tunnel with a

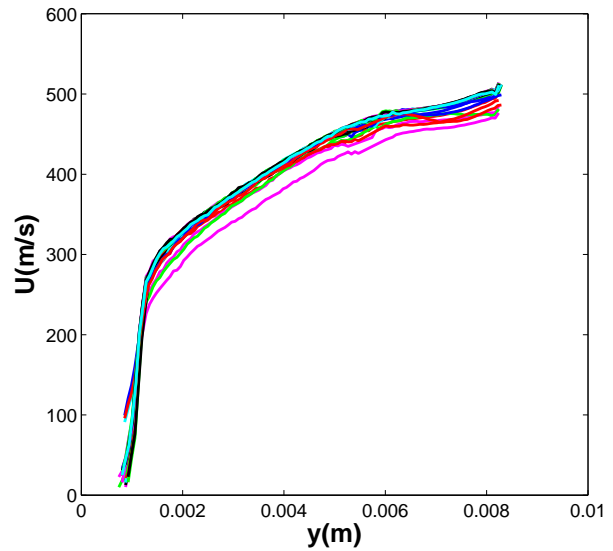


Figure 6. Velocity profiles 3mm downstream of the compression corner for 25 perturbed cases

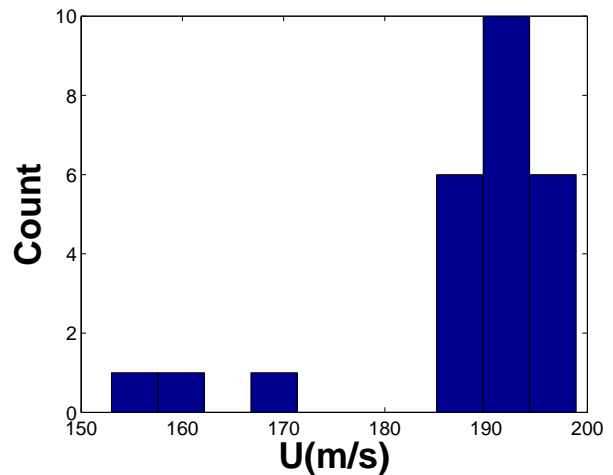


Figure 7. Histogram of system response to perturbations 1mm above the compression corner

small 20° compression ramp. The interaction zone was significantly altered by the small height of the wedge, as the resulting shock structure was weaker than the inviscid predictions. The maximum measured flow turning angle was $\approx 8^\circ$, and the shock angle was $\approx 37^\circ$.

Geometric perturbations were placed upstream of the compression corner on the wall opposite the wedge. These perturbations had a significant effect on the flow. In the perturbed cases, the interaction zone extended further from the compression corner in both the streamwise and wall-normal directions. Velocity profiles show that the sensitivity of the flow is a strong spatial function. Histograms of the system response at a single point provide a possible metric for quantitative comparison between the experiment and stochastic sim-

ulations. Numerous other metrics can be extracted from the data, including the location of the primary shock, the projection of the shock to the wall, and full velocity field comparisons for individual perturbation configurations.

4 ACKNOWLEDGEMENTS

This material is based upon work supported by the Department of Energy [National Nuclear Security Administration] under Award Number NA28614. Support was also received from the Graduate Research Fellowship Program of the National Science Foundation and the National Defense Science and Engineering Graduate Fellowship program of the Department of Defense.

REFERENCES

- Beresh, S., Clemens, N., and Dolling, D., 2002, "Relationship between upstream turbulent boundary-layer velocity fluctuations and separation shock unsteadiness," *AIAA Journal*, Vol. 40, pp. 2412-2422.
- Blinde, P., Humble, R., van Oudheusden, B., and Scarano, F., 2009, "Effects of micro-ramps on a shock wave/turbulent boundary layer interaction," *Shock Waves*, Vol. 19, pp. 507-520.
- Bookey, P., Wyckham, C., Smits, A., and Martin, M., 2005, "New experimental data of STBLI at DNS/LES accessible Reynolds numbers," *AIAA Paper* 2005-309.
- Dolling, D.S., 2001, "Fifty years of shock-wave/boundary-layer interaction research: What next?," *AIAA Journal*, Vol. 39, pp.1517-1531.
- Ganapathisubramani, B., Clemens, N., and Dolling, D., 2007, "Effects of upstream boundary layer on the unsteadiness of shock-induced separation," *Journal of Fluid Mechanics*, Vol. 585, pp. 369-394.
- Helmer, D., Campo, L., and Eaton, J., 2011, "Three-dimensional features of a Mach 2.1 Shock/Boundary Layer Interaction," Submitted to the *Journal of Fluid Mechanics*.
- Hou, Y., Clemens, N., and Dolling, D., 2003, "Wide-field piv study of shock-induced turbulent boundary layer separation," *AIAA Paper* 2003-0441.
- Humble, R., Scarano, F., and van Oudheusden, B., 2007, "Particle image velocimetry measurements of a shock wave/turbulent boundary layer interaction," *Experiments in Fluids*, Vol. 43, pp. 173-183.
- Humble, R., Elsinga, G., Scarano, F., and van Oudheusden, B., 2009, "Three-dimensional instantaneous structure of a shock wave/turbulent boundary layer interaction," *Journal of Fluid Mechanics*, Vol. 622, pp. 33-62.
- Piponniau, S., Dussauge, J., Debieve, J., and Dupont, P., 2009, "A simple model for low-frequency unsteadiness in shock-induced separation," *Journal of Fluid Mechanics*, Vol. 629, pp. 87-108.
- Selig, M., and Smits, A., 1991, "Effect of periodic blowing on attached and separated supersonic turbulent boundary layers," *AIAA Journal*, Vol. 29, pp. 1651-1658.
- Smits, A., and Muck, K., 1987, "Experimental study of three shock wave/turbulent boundary layer interactions," *Journal of Fluid Mechanics*, Vol. 182, pp. 291-314.
- Souverein, L., and Debieve, J., 2010, "Effect of air jet vortex generators on a shock wave boundary layer interaction," *Experiments in Fluids*, Vol. 49, pp. 1053-1064.
- Souverein, L., Dupont, P., Debieve, J., Dussauge, J., van Oudheusden, B., and Scarano, F., 2010, "Effect of interaction strength on unsteadiness in turbulent shock-wave induced separations," *AIAA Journal*, Vol. 48, pp. 1480-1493.